Family of prokaryote cyclic nucleotide-modulated ion channels

Marijke Brams[a,1], Jana Kusch[b,1], Radovan Spurny[a], Klaus Benndorf[b], and Chris Ulens[a,2]

[a]Laboratory of Structural Neurobiology, Department of Cellular and Molecular Medicine, Katholieke Universiteit Leuven, B-3000 Leuven, Belgium; and [b]Institute of Physiologie II, University Hospital Jena, 07743 Jena, Germany

Edited by Christopher Miller, Howard Hughes Medical Institute, Brandeis University, Waltham, MA, and approved April 15, 2014 (received for review February 4, 2014)

Cyclic nucleotide-modulated ion channels are molecular pores that mediate the passage of ions across the cell membrane in response to cAMP or GMP. Structural insight into this class of ion channels currently comes from a related homolog, MloK1, that contains six transmembrane domains and a cytoplasmic cyclic nucleotide binding domain. However, unlike eukaryote hyperpolarization-activated cyclic nucleotide-modulated (HCN) and cyclic nucleotide-gated (CNG) channels, MloK1 lacks a C-linker region, which critically contributes to the molecular coupling between ligand binding and channel opening. In this study, we report the identification and characterization of five previously unidentified prokaryote homologs with high sequence similarity (24–32%) to eukaryote HCN and CNG channels and that contain a C-linker region. Biochemical characterization shows that two homologs, termed AmaK and SthK, can be expressed and purified as detergent-solubilized protein from *Escherichia coli* membranes. Expression of SthK channels in *Xenopus laevis* oocytes and functional characterization using the patch-clamp technique revealed that the channels are gated by cAMP, but not cGMP, are highly selective for K^+ ions over Na^+ ions, generate a large unitary conductance, and are only weakly voltage dependent. These properties resemble essential properties of various eukaryote HCN or CNG channels. Our results contribute to an understanding of the evolutionary origin of cyclic nucleotide-modulated ion channels and pave the way for future structural and functional studies.

cyclic AMP | cyclic GMP | electrophysiology | protein purification

Hyperpolarization-activated cyclic nucleotide-modulated (HCN) and cyclic nucleotide-gated (CNG) channels belong to the superfamily of voltage-gated K^+ channels. Both types of channels share a similar domain topology with six transmembrane domains, a C-linker region, and a cyclic nucleotide binding domain (CNBD). The S5–S6 segment forms the channel pore, including the selectivity filter for cations. The S4 segment contains several positively charged amino acids, suggesting that it acts as voltage sensor. Despite these similarities in sequence, the function of HCN and CNG channels is noticeably different: HCN channels activate upon membrane hyperpolarization and can be modulated by cyclic nucleotides. They are weakly selective for K^+ over Na^+ ions (for reviews, see refs. 1–3). In contrast, CNG channels are activated by the binding of cyclic nucleotides solely and their activity depends only weakly on voltage. The ionic current is carried by both monovalent and divalent cations (for reviews, see refs. 4 and 5).

Insight into the structure of HCN channels has been gained only from crystal structures of the isolated intracellular C-linker and CNBD of mammalian HCN1, HCN2, HCN4, and invertebrate spHCN1. These parts of the channel assemble into tetramers (6–9). Further structural information comes from prokaryote ion channels that are homologous to HCN and CNG channels, such as the bacterial cyclic nucleotide-regulated K^+ channel MloK1 (10–13). MloK1 lacks a C-linker region, but has a CNBD with an overall structure that is remarkably similar to the CNBD of eukaryote HCN channels (10). Based on the dimer assembly of the MloK1 CNBD in the crystal structure, a gating mechanism has been proposed in which the pore opening in the tetrameric channel arises from the action of the four CNBDs as a dimer of dimers (10). The crystal structure of the MloK1 transmembrane domain (11) reveals a domain topology that resembles that of the voltage-gated K^+ channel Kv1.2 (14), but with important differences. The MloK1 structure suggests that the S1–S4 domain and its associated linker in MloK1 can serve as a clamp to constrain the gate and possibly function in concert with the CNBD to regulate channel opening (11). Additionally, crystal structures have also been determined for the C-linker and cyclic nucleotide binding homology domain (CNBHD) of related ion channels, including the zebrafish EAG-like (ELK) K^+ channel (15), the mosquito ERG K^+ channel (16), and the mouse EAG1 K^+ channel (17). Structural insight into the mechanism of ion permeation has been derived from a prokaryote ion channel NaK (18), which was mutated to mimic the CNG channel pore region (19). Collectively, these structural data have brought valuable information about the determinants of ion permeation, domain assembly, ligand recognition, channel gating and regulation, as well as effects of disease-causing mutations (20).

Despite this tremendous progress, crystal structures for whole-eukaryote HCN and CNG channels are still not available at present, and structural insight into fundamental aspects of ion channel function is still lacking, such as the inverse voltage sensitivity in HCN channels and the coupling between cyclic nucleotide binding and channel opening by the C-linker domain, which is, as mentioned, absent in the MloK1 channel (10). In contrast, a putative voltage-gated K^+ channel containing a C-linker region and CNBD similar to eukaryote channels was identified in the genome of the cyanobacterium *Trichodesmium*

Significance

We describe a previously unidentified family of prokaryote cyclic nucleotide-modulated ion channels. In eukaryotes, CNG channels play important roles in signal transduction as they mediate the passage of ions across the cell membrane in response to cAMP or cGMP. In this study, we demonstrate that two prokaryote homologs, AmaK and SthK, can be expressed and purified from *Escherichia coli* membranes. We reveal that SthK has functional properties that closely resemble eukaryote HCN or CNG channels. SthK is gated by cyclic AMP, but not cyclic GMP, and selects K^+ over Na^+ ions in a weakly voltage-dependent manner. Our results contribute to understanding the evolutionary origin of cyclic nucleotide-modulated ion channels and pave the way for future structural and functional studies.

Author contributions: M.B., J.K., K.B., and C.U. designed research; M.B., J.K., and R.S. performed research; M.B. and J.K. contributed new reagents/analytic tools; M.B., J.K., R.S., K.B., and C.U. analyzed data; and J.K., R.S., K.B., and C.U. wrote the paper.

The authors declare no conflict of interest.

This article is a PNAS Direct Submission.

Freely available online through the PNAS open access option.

[1]M.B. and J.K. contributed equally to this work.

[2]To whom correspondence should be addressed. E-mail: chris.ulens@med.kuleuven.be.

This article contains supporting information online at www.pnas.org/lookup/suppl/doi:10.1073/pnas.1401917111/-/DCSupplemental.

erythraeum (21), here termed TerK, and it was suggested to possibly represent an ancestral HCN or CNG channel (21). However, neither structure nor function of this prokaryote homolog is known. In this study, we report the characterization of TerK and four additional prokaryote ion channels, which all contain six putative transmembrane domains, a C-linker region, and a CNBD, and apparently form a family of prokaryote ion channels with close similarity to eukaryote HCN and CNG channels. We describe the expression in *Escherichia coli*, detergent screening and biochemical purification of these different homologs. Moreover, we identified two homologs, SthK (from *Spirochaeta thermophila*) and AmaK (from *Arthrospira maxima*), which can be stably extracted with detergents and purified in sufficiently high amounts for biochemical and structural studies. Using confocal fluorescence microscopy and electrophysiological recordings, we describe essential functional properties of one homolog, SthK. We find that SthK has electrophysiological properties that closely resemble those of eukaryote CNG channels as it is gated by intracellular cAMP and produces large unitary currents, whereas its activity is relatively insensitive to voltage. However, unlike CNG channels, SthK contains the selectivity filter sequence -TIGYGD-, which is more similar to HCN channels and other K^+ selective channels. We could experimentally demonstrate that SthK channels are highly selective for K^+ over Na^+ ions. Importantly, SthK has several sequence features that closely resemble eukaryote cyclic nucleotide-modulated channels, including a C-linker region, which is missing in previously studied prokaryote homologs, such as MloK1 (10, 12, 13) and MmaK (22). Together, these data make the SthK channel a promising candidate for future structural analysis to learn more about how mammalian CNG and HCN channels work.

Results

Bioinformatics and Sequence Analysis. To identify suitable candidates for biochemical and structural studies on HCN and CNG channels, we screened the bacterial genome database of the National Center of Biotechnology Information (http://blast.ncbi.nlm.nih.gov/) using a standard BLASTP search (23) and the human HCN2 channel sequence as a template. Several ORFs with significant sequence identity to HCN2 (more than 24%) were identified in several species, including *Trichodesmium erythraeum* IMS101 (TerK), which was previously identified in another study (21), as well as *Arthrospira maxima* CS-328 (AmaK), *Lyngbya* sp. PCC 8106 (LpcK), *Spirochaeta thermophila* DSM 6192 (SthK), and *Leptospira biflexa* serovar Patoc strain (LbiK). Among these species, *Trichodesmium*, *Arthrospira*, and *Lyngbya* belong to the genus of cyanobacteria or blue-green algae, whereas *Spirochaeta thermophila* is an extremely thermophilic bacterium (24) and *Leptospira biflexa* is a saprophytic pathogen (25). Alignment of these sequences using ClustalW (26) and further inspection revealed structural motifs that are common among members of the superfamily of voltage-gated K^+ channels (Fig. 1*A*). All identified bacterial sequences contain six putative transmembrane domains (S1–S6), the K^+-selectivity signature sequence T-V/I-GYG in the selectivity filter (SF) region, and a putative voltage sensor (S4) characterized by the sequence R/Kxx-Rxx-Rxx-Rxx-R/Kxx-R, where every third residue is positively charged (arginine or lysine) and x is in most cases a hydrophobic residue (a full sequence alignment is shown in Fig. S1). Not all arginine or lysine residues are conserved in each homolog as they range from two positive charges in SthK to five positive charges in LbiK. Similar to eukaryote HCN and CNG channels, the carboxyl-terminal region of the bacterial sequences contain a CNBD connected to the transmembrane region via a C-linker. In contrast to the eukaryote channels, the bacterial channels contain only a very short amino-terminal sequence. The evolutionary relationship of these bacterial homologs is further illustrated in a phylogenetic tree (Fig. 1*C*) and a pairwise sequence identity diagram (Fig. 1*D*). The sequence identity among the different bacterial homologs varies between

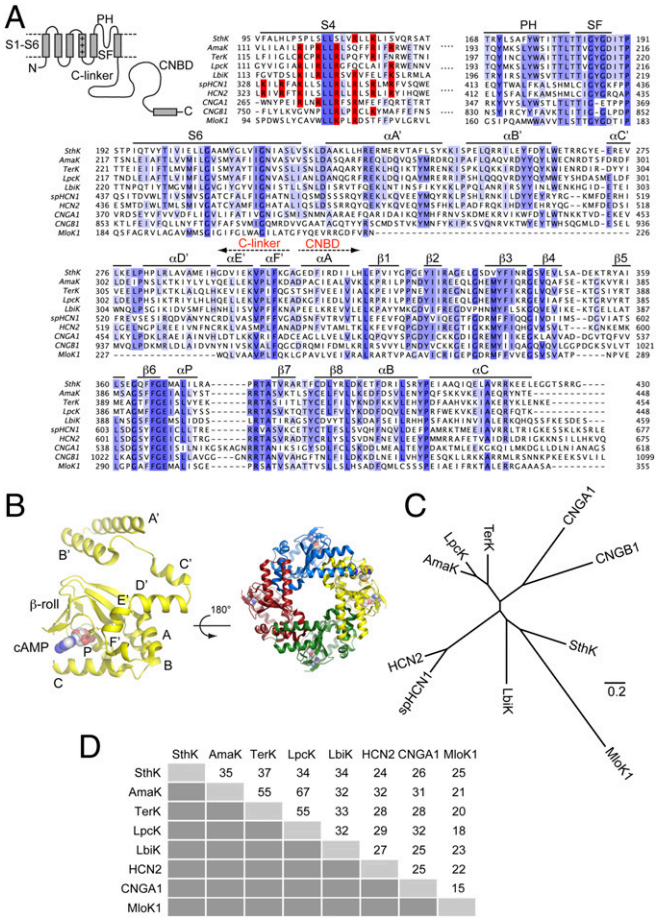

Fig. 1. Sequence analysis of prokaryote cyclic nucleotide-modulated ion channels. (*A*) Sequence alignment of five prokaryote homologs with spHCN1, human HCN2, human CNGA1, human CNGB1, and MloK1. The cartoon represents the transmembrane topology of a single-channel subunit. In the S4 segment, positively charged residues are colored in red. Residues are colored in shades of blue by using an identity threshold of 50%. Sequence features are annotated according to the secondary structures features described in the X-ray crystal structure of the HCN2 C-linker region (A′–F′) and cyclic nucleotide binding domain (A–C) (6). (*B*) Cartoon representation of the HCN2 C-linker region and cyclic nucleotide binding domain (6). The left panel is a single subunit, and the right panel is a tetrameric assembly. cAMP molecules are shown as spheres (white, carbon; red, oxygen; blue, nitrogen; orange, phosphor). (*C*) Phylogenetic relationship of the homologs described in *A*. (*D*) Pairwise sequence identities of the homologs described in *A*.

32% (AmaK compared with LbiK) and 67% (AmaK compared with LpcK). Compared with human HCN2, the sequence identity varies between 24% for SthK and 32% for AmaK. Compared with human CNGA1, the sequence identity varies between 25% for LbiK and 32% for LpcK. These results indicate that the newly identified homologs could be more suitable to serve as a model for HCN and CNG channels than the previously identified MloK1 channel (10–13), which has only 22% sequence identity with HCN2 (15% with CNGA1) and essentially lacks the C-linker region. Together, these data demonstrate the existence of putative cyclic nucleotide-modulated ion channels in certain bacteria, with marked similarity to HCN and CNG channels as they contain six transmembrane domains connected to a CNBD via a C-linker region.

Expression and Detergent Screening in *E. coli*. Next, we investigated whether the five newly identified HCN/CNG channel homologs could be expressed in *E. coli*. To facilitate this study, we

expressed these homologs from synthetic genes cloned into the vector pWaldo-GFPe (27), which covalently couples GFP-Hisx8 to the carboxyl-terminal end of the target protein (Fig. 2*A*). We transformed each homolog into BL21(DE3), C41(DE3), C43 (DE3), and their pLysS variant strains, and measured whole-cell fluorescence as an initial marker for protein expression. As a positive control, we used the prokaryote K^+ channel construct KcsA-GFP, which is robustly expressed in *E. coli*. We observed that AmaK-GFP could be expressed at fluorescence levels of 21% in C43(DE3) and 44% in C41(DE3) compared with KcsA-GFP in BL21(DE3) (Fig. 2*B*). No fluorescence significantly higher than background could be observed for the other homologs, except for SthK-GFP, which expressed at ~20% in C41 (DE3) compared with KcsA-GFP.

Next, we conducted a detergent screen to identify detergents that extract AmaK-GFP and SthK-GFP from the membrane in an oligomeric and monodisperse state. We used fluorescence size exclusion chromatography (FSEC) (28) on crude membranes solubilized with a range of different detergents, namely CYMAL-6, lauryldimethylamine *N*-oxide (LDAO), octyl glucoside (OG), nonylglucoside (NG), octylmaltoside (OM), Fos-choline-12 (Fos-12), decylmaltoside (DM), undecylmaltoside (UDM), dodecylmaltoside (DDM) and tridecylmaltoside (TDM), lauryl maltose neopentyl glycol (LMNG), C12E9, CHAPS, and HEGA-10. The FSEC method relies on the identification of a symmetric peak running between the void volume of the size exclusion column (~7 mL) and the elution volume of free GFP (~18 mL). For example, the positive control KcsA-GFP behaves as a stable tetramer in a range of different detergents (29) and elutes as an intense symmetric fluorescent peak at 14.5 mL after solubilization with UDM (Fig. 2*C*). For AmaK-GFP, we also identified UDM as a suitable detergent because the FSEC profile shows a symmetric peak with a retention volume of 12.7 mL (Fig. 2*D*). Furthermore, we used in-gel fluorescence of nickel affinity-purified AmaK-GFP and observed a fluorescent band near the 50-kDa marker, which likely corresponds to monomeric AmaK-GFP (81 kDa). This phenomenon of gel shifting is commonly observed for membrane proteins and can be explained by the higher number of SDS molecules absorbed compared with water-soluble globular proteins (30). Additionally, we also observed a weaker fluorescent band between the 100 and 150 kDa marker, indicating that an oligomeric assembly of AmaK-GFP, possibly dimers, is partially stable in SDS. For SthK, we identified DDM as a suitable detergent and observed an FSEC profile similar to AmaK-GFP. SthK-GFP elutes as a symmetric peak with a retention volume of 13.4 mL (Fig. 2*E*). The in-gel fluorescence of nickel affinity-purified SthK-GFP shows a single band near the 50-kDa marker, which is similar to AmaK-GFP. In addition, for AmaK and SthK several other hits were obtained from our detergent screen, including Fos-choline-12, HEGA-10, and LMNG (Fig. S2). Together, these results demonstrate that two prokaryote HCN/CNG channel homologs, namely AmaK and SthK, can be expressed in *E. coli* and extracted from membranes in a monodisperse state. These results pave the way for large-scale production, biophysical characterization, and crystallization screening.

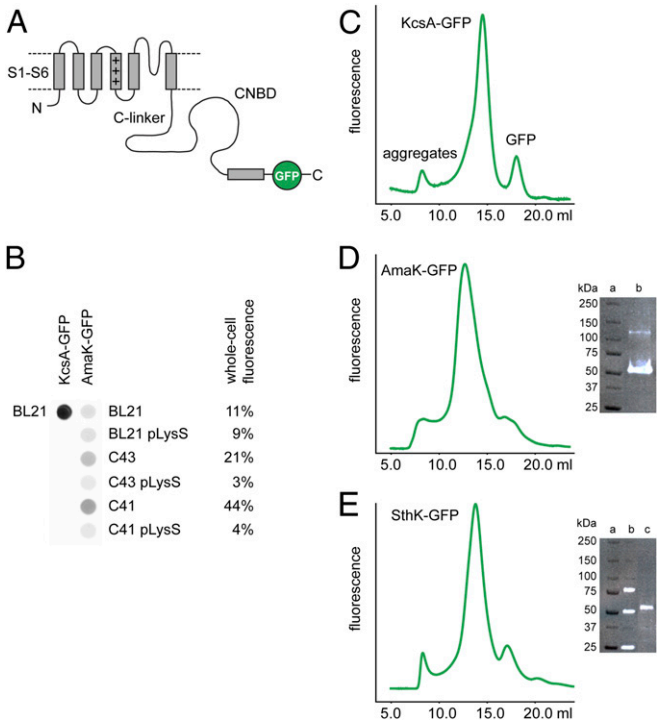

Fig. 2. Biochemical characterization of prokaryote cyclic nucleotide-modulated ion channels. (*A*) Cartoon presentation of the C-terminal GFP-fusion constructs used for detergent screening. (*B*) Whole-cell fluorescence obtained from *E. coli* cultures expressing AmaK-GFP in different strains. Fluorescence intensity was normalized relative to KcsA-GFP (29). (*C*) FSEC profile (28) of KcsA-GFP after solubilization with 2% (wt/vol) undecylmaltoside and gel filtration in running buffer containing 0.15% undecylmaltoside. (*D*) FSEC profile of AmaK-GFP after solubilization under the same conditions as in *C*. The gel scan shows in-gel green fluorescence of His-trap purified protein (lane b) loaded on a 4–15% Miniprotean TGX gel. Lane a contains Precision Plus All Blue standard from Bio-Rad. (*E*) FSEC profile of SthK-GFP after solubilization with 2% dodecylmaltoside and gel filtration in running buffer containing 0.05% dodecylmaltoside. The gel scan shows in-gel green fluorescence under the same conditions as in *D* except that an additional ladder (Fluorescent WesternC standard from Bio-Rad) was loaded in lane b. Lane c was loaded with His-trap purified protein.

Membrane Localization and Functional Characterization. To test whether SthK and AmaK can be studied in a heterologous expression system suitable for electrophysiological experiments, we tried to functionally express SthK and AmaK GFP-fusion constructs in *Xenopus laevis* oocytes.

First, we used confocal fluorescence microscopy to whole intact oocytes and investigated whether or not SthK-GFP localizes at the cell membrane, i.e., in the periphery of the oocyte. To visualize the boundaries of the cell membrane, we incubated oocytes in a bath solution containing 5 μM Alexa Fluor 633-labeled wheat germ agglutinin (WGA-Alexa 633), a compound that labels the extracellular face of the plasma membrane. Exposure to 633-nm laser light resulted in bright red fluorescence in the periphery of both SthK-GFP–injected and control oocytes (Fig. S3). In parallel, the WGA-labeled oocytes were exposed to 488-nm laser light, resulting in a bright green fluorescence signal only in SthK-GFP–expressing oocytes (Fig. S3 *A* and *B*) but not in control oocytes (Fig. S3 *C* and *D*). Additionally, the emission spectrum of SthK-GFP obtained by spectral imaging (*SI Experimental Procedures*) is clearly different from oocyte autofluorescence and perfectly superimposes with the emission spectrum obtained from GFP expressed in HEK cells (*SI Experimental Procedures*; Fig. S4). Together, these results indicate that SthK-GFP is expressed in or near the membrane of the oocytes.

To gain further arguments that SthK-GFP is expressed in the plasma membrane and not only in submembranal compartments, we quantified the degree of overlap of the SthK-GFP fluorescence with WGA-Alexa 633 fluorescence at higher magnification. It was observed previously that the construct CNGB1b-TFP:CNGA2:CNGA4, a heterotetrameric eukaryotic CNG channel that produces reliable trafficking to the membrane as confirmed by current recordings, yields a degree of overlap of ~54% between the fluorescence signal for TFP and WGA-Alexa 633 (31). The average fluorescence profiles perpendicular to the plasma membrane yielded a degree of overlap of 65.3 ± 4.43% (n = 3) between GFP and WGA-Alexa 633 fluorescence (Fig. S3*B*). This result even exceeds the degree of overlap observed

PHYSIOLOGY

in the experiment with CNGB1b-TFP:CNGA2:CNGA4 and therefore suggests significant membrane localization of SthK-GFP. As previously noted by Nache et al. (31), these results should be interpreted with caution because staining the membrane of control oocytes produced a profile with a half-maximum width of 2.0 ± 0.15 μm (n = 3) (Fig. S3*D*), which by far exceeds the microscope resolution (0.3 mm) and typical membrane thickness of ∼3–4 nm. The result can be explained by the extensive folding of the oocyte membrane (31). Despite this optical limitation, our confocal fluorescence microscopy experiments indicate that SthK-GFP produces significant green fluorescence at the oocyte membrane and suggests that SthK-GFP localizes to the cell membrane. Performing the same experiments with AmaK-GFP did not result in GFP-related fluorescence signals, indicating that there is no expression of this construct in the oocyte membrane. Spectral images comparing AmaK-GFP with SthK-GFP injected oocytes are shown in Fig. S5.

Channel Gating. We first tried to record whole-cell currents by using the two-electrode voltage-clamp technique. The result was negative, suggesting that SthK channels are not functional or have a gating mechanism that is different to eukaryote HCN channels. Next, we used the patch-clamp technique with patches in the inside-out configuration, which allows the investigator to apply molecules to the internal face of the membrane. Because SthK carries the -TIGYGD- selectivity filter sequence in the pore loop, suggesting a channel that selects K^+ over Na^+ ions, the following experiments were performed in symmetrical solutions containing 150 mM K^+. In patches containing presumably many SthK channels (macropatches), the application of cAMP (500 μM) to the bath solution produced robust current responses at positive and negative voltages when applying a voltage ramp from −130 to +130 mV (Fig. 3). Such a response was not observed in the absence of cAMP (Fig. 3*A*) or in patches from uninjected control oocytes. This result suggests a gating mechanism for SthK similar to eukaryote CNG channels, which can be activated by cyclic nucleotides and which are relatively insensitive to voltage. The cAMP-evoked current through SthK channels was reversible when removing the cAMP and the amplitude was stable after an initial run-up of tens of seconds following the cAMP application. There was no indication for any inactivation or desensitization in the presence of cAMP.

Next, we studied the cAMP sensitivity of SthK channels in greater detail. Fig. 3*B* shows the concentration–activation relationship recorded at 150 mM symmetrical K^+ solution. Fit of the data points with Eq. **S1** yielded the cAMP concentration of half-maximum activation, EC_{50}, of 3.68 ± 0.55 μM and the Hill coefficient, H, of 1.33 ± 0.08 (n = 10). The Hill coefficient larger than unity indicates that the subunits cooperate upon channel activation.

Notably, we did not observe any current response when applying cGMP instead of cAMP (Fig. 3 *A* and *C*). To test whether cGMP is not able to bind to the SthK binding domain or acts as a competitive antagonist, we applied 3 μM cAMP, a concentration near the EC_{50} value, together with 5 mM cGMP (Fig. 3*C*). Under this condition, cAMP is not able to activate the channel, indicating a competition of cGMP and cAMP at the binding site. Thus, cGMP acts as a competitive antagonist, which is remarkable, because both cAMP and cGMP are agonists in most of the cyclic nucleotide-modulated ion channels described so far.

Ion Selectivity. To confirm the predicted selectivity of K^+ over Na^+, we applied voltages from −100 to +100 mV in 20-mV steps at 500 μM cAMP with either 150 mM KCl or NaCl in the bath and the pipette solution, respectively. The resulting current–voltage relations and representative current traces for each case are shown in Fig. 4*A*. The results demonstrate that SthK channels allow K^+ but not Na^+ ions to permeate, similar to the prokaryotic cyclic nucleotide-gated K^+ channel MmaK (22) and MloK1 (13). At symmetrical potassium, there is only weak outward rectification. This resembles the voltage dependence of eukaryotic CNG channels under symmetrical conditions (32, 33).

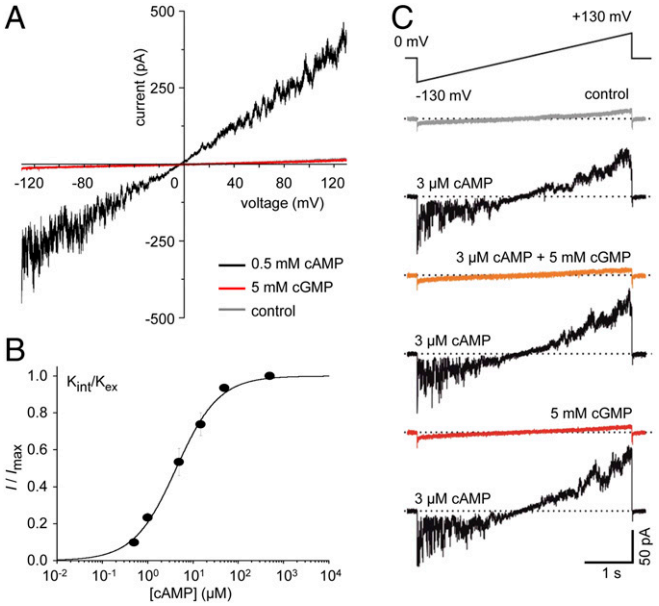

Fig. 3. Ligand selectivity in inside-out macropatches. (*A*) A voltage ramp ranging from −130 to +130 mV in 4.5 s was applied to an inside-out macropatch excised from a SthK-GFP–expressing *Xenopus laevis* oocyte. The black trace represents the current response after applying 500 μM cAMP at symmetrical potassium. There was no current response after removal of cAMP or applying 5 mM cGMP to the same patch, shown as gray and red traces, respectively. (*B*) The concentration–activation relationship for cAMP was obtained at symmetrical potassium. Means were calculated from 3 to 14 recordings. Error bars indicate SEM. The black curve is the best fit of the mean values using Eq. **S1**. When fitting single recordings, we obtained the following: EC_{50} = 3.68 ± 0.55 μM (n = 10), H = 1.33 ± 0.08 (n = 10). (*C*) A voltage ramp under similar conditions as described in *A* was applied to an inside-out macropatch. The representative traces show current responses after applying 3 μM cAMP (black traces), 3 μM cAMP plus 5 mM cGMP (orange trace), or 5 mM cGMP (red trace). The ligands were washed in the same order as shown. There was no current response as long as cGMP was applied.

Single-Channel Properties. We also studied the activity of single SthK channels. Fig. 4*B* shows a representative example of current traces and the corresponding amplitude histogram. The amplitude of the single-channel current at +100 mV was 7.1 ± 0.4 pA (n = 4), resulting in a single-channel conductance of 71 pS. This value is in the upper range of reported values for eukaryote CNG channels (20–80 pS) (reviewed in ref. 4), but is much higher than that in eukaryotic HCN channels, which have an extremely low single-channel conductance of only 1–2 pS (34–36). The probability for one channel to be open, P_o, at saturating ligand concentration was 13.8 ± 1.72% (n = 3), which is low compared with the respective P_o values in eukaryotic CNGA1 (94.0%) (37), CNGA2 (99.0%) (38), and HCN2 (>99%) (36) channels.

Discussion

Only a few prokaryotic ion channels have been successfully expressed in *Xenopus laevis* oocytes as heterologous expression system, including the mechanosensitive channel MscS (39), a proton-gated ion channel from the nicotinic acetylcholine receptor family (40), or an ATP-sensitive K^+ channel (41). Bacterial CNG channels could only be successfully studied as reconstituted proteins in liposomes (13, 42) or in giant *E. coli* spheroplasts (22). In the present study, fluorescence imaging and electrophysiological patch-clamp recording demonstrated that SthK-GFP can be expressed as a functional ion channel protein

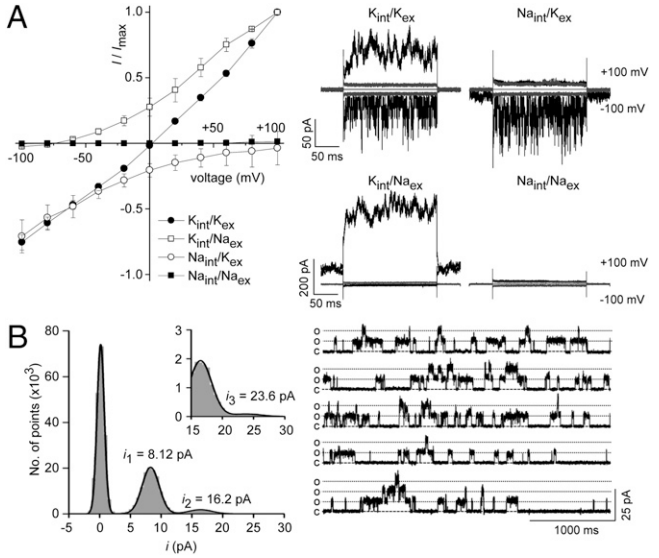

Fig. 4. Functional characteristics of SthK in inside-out patches. (*A*) (*Left*) Current–voltage relationship as measured under four different ionic conditions. Bath solution and pipette solution contained either K^+ or Na^+ ions, respectively. The bath solution additionally contained a saturating cAMP concentration of 500 μM. Positive values indicate outward currents, and negative values indicate inward currents. Current amplitudes are normalized to the maximum value obtained at +100 mV at K_{int}/K_{ex} and K_{int}/Na_{ex}, respectively. Means were calculated from three to nine patches. Error bars indicate SEM. (*Right*) Representative currents (black traces: at 500 μM cAMP; gray traces: no cAMP) for each of the four ionic conditions. (*B*) Single-channel events were recorded at a saturating concentration of 500 μM cAMP at symmetrical potassium and +100 mV. (*Left*) Representative current–amplitude histogram for a three-channel patch. The main histogram was fitted by the sum of three Gaussian functions (for one closed and two open levels) (black line). The amplitude of the single-channel current was determined to be 8.1 pA (with a SD obtained from the Gaussian fit of 0.02 pA). The *Inset* shows the same histogram at higher magnification to visualize the third open level peak. This histogram was fitted by the sum of two Gaussian functions (black line). (*Right*) Shown are representative traces from the same recording as shown in the left panel. Closed and open levels are indicated as dashed (c) and dotted lines (o).

in the plasma membrane of *Xenopus* oocytes. We investigated functional parameters of SthK channel gating in excised inside-out macropatches to learn about its relationship to other members of the family of cyclic nucleotide-modulated ion channels.

Most of the prokaryotic and eukaryotic cyclic nucleotide-gated channels are sensitive to both cAMP and cGMP, very often preferring one ligand over the other (4, 43). It has been shown that, regardless of ligand preference, a highly conserved arginine (Arg618 in human HCN2 or Arg561 in human CNGA1) in the CNBDs of eukaryotic (6) and prokaryotic cyclic nucleotide-modulated channels (13) as well as other cyclic nucleotide-dependent proteins (44) is essential for cNMP binding. Mutating this arginine to glutamate decreased the affinity for cNMP dramatically in both eukaryotic CNG and HCN channels (45, 46). A similar effect was observed when neutralizing this residue in the prokaryotic MloK1 (42). Interestingly, this conserved arginine is also present in the sequences of all prokaryotic channels described in our study (Fig. 1), indicating that all these homologs are able to bind cyclic nucleotides.

Channels that bind both cAMP and cGMP have an amino acid residue next to this arginine, which provides a hydroxyl group: a threonine in eukaryotic channels (6) and a serine in MloK1 (13). In SthK, there is a threonine at that very position, arguing for a binding of both cyclic nucleotides. Another arginine residue, which has been described to be important for both cGMP and cAMP binding resides in the C-helix of the binding pocket (Arg348 in MloK1) (47). This arginine was also found in the SthK sequence. Herein, we showed that, as expected from the sequence, indeed both cAMP and cGMP do bind to the SthK CNBD, however, with opposite effects on channel gating: While binding of cAMP activated SthK channels, cGMP binding did not. This is remarkable because to our knowledge it is the first time that an antagonistic effect of a cNMP to a CNG/HCN channel homolog has been demonstrated. However, the idea that cGMP can act differently than as a pure agonist has been proposed earlier for catfish CNGA2. Young and co-workers described a so-called bimodal agonism, meaning that cGMP exhibits two opposite modes of action: "pro action" that enhances receptor activation and "con action" that suppresses activation (48–50). It would be interesting to investigate whether there is any analogy in the fCNGA2 bimodal agonism and the cGMP antagonism found herein.

The sequence of the SthK pore region contains a TIGYGD motif in the selectivity filter, arguing for a K^+-selective channel. Our experimental results confirmed this prediction: SthK channels allow K^+ but not Na^+ to permeate in both inward and outward direction (Fig. 4*A*). A similar ion selectivity was described for other bacterial CNG channels, such as MloK1 (13) and MmaK (22).

The activation mechanism of the different types of cyclic nucleotide-modulated channels is different. Eukaryote CNG channels strictly depend on the binding of cyclic nucleotides and are only weakly voltage dependent. In contrast, eukaryote HCN channels require hyperpolarizing voltages for activation and are only modulated by cyclic nucleotides. In our study, we show at symmetrical K^+ that SthK is only weakly voltage dependent, which resembles the behavior of eukaryotic CNG channels (32, 33). One possible explanation for the lack of voltage dependence in SthK could be the relatively low number of three positively charged residues in the intracellular half of the S4 domain. In comparison, voltage-dependent eukaryote HCN channels have seven positively charged residues within S4. In addition to S4, the secondary structure of the S4–S5 linker was also shown to play an important role for voltage sensing (51, 52). In voltage-dependent K^+ channels, this linker is a relatively rigid α-helix, transferring the voltage-induced conformational changes of the S4 to the channel gate (51). For eukaryotic CNG channels, it was suggested that the S4–S5 linker is unable to transfer this conformational change as it is a short and flexible loop, making the channel independent of voltage (52). Similar to CNGA1–4 isoforms, the specific amino acid composition of the S4–S5 linker in SthK predicts a flexible loop rather than a rigid α-helix (see full sequence in alignment in Fig. S1). Additionally, the S4–S5 linker in SthK contains the structure-breaking amino acid proline at position 132, which is conserved in almost all eukaryotic CNGA1–4 subunits of different species and which is suggested to significantly participate in making the S4–S5 linker unable to transfer S4 movements to the pore (52).

In summary, several sequence motifs of SthK channels resemble those in eukaryote CNG channels and therefore suggest similarity in function. Certain key amino acids in the cyclic nucleotide binding domain as well as the S4–S5 linker are conserved between SthK and eukaryote CNG channels. In agreement with this conservation, our electrophysiological experiments demonstrate that SthK is gated by the intracellular application of cAMP. However, unlike eukaryote CNG channels, SthK channels contain a sequence in the selectivity filter that resembles HCN channels and other K^+-selective channels but not CNG channels. Our functional characterization indeed confirms that SthK is a K^+-selective channel. Importantly, SthK and all of the other homologs described in our study contain a C-linker region, which is absent in previously studied prokaryote homologs, including MloK1 and MmaK. This observation might contribute to a better understanding of the evolutionary origin of CNG channels and suggests that an ancestral CNG-HCN gene may have arisen already in the bacterial stage of evolution. Finally, our biochemical data demonstrate that SthK and AmaK can be expressed and

purified in quantities sufficient for future biochemical and structural studies. If available, X-ray crystal structures of SthK and AmaK, most desirably in the absence and presence of cyclic nucleotides, may bring essential progress for our understanding of the channel gating, because these bacterial channels do contain the C-linker region.

Experimental Procedures

LpcK, TerK, SthK, LbiK, and AmaK were expressed as C-terminal GFP fusions using the vector pWaldo-GFPe or pGEM-HE for expression in *E. coli* or *Xenopus* oocytes, respectively. Confocal fluorescence microscopy was used to determine protein localization in the membrane. Patch-clamp recordings were carried out in the inside-out configuration. Full methods are described in *SI Experimental Procedures*.

ACKNOWLEDGMENTS. We thank Damian Bell and Ralf Schmauder for generous feedback on the manuscript. cDNA encoding KcsA was a gift from Roderick MacKinnon (Rockefeller University). pWaldo-GFPe was a gift from Jan-Willem de Gier (Stockholm University). This work was supported by Fonds Wetenschappelijk Onderzoek–Vlaanderen Grants G.0739.09, G.0743.10, G.0939.11, and G.0762.13, and Onderzoekstoelage OT/13/095 (to C.U.).

1. Robinson RB, Siegelbaum SA (2003) Hyperpolarization-activated cation currents: From molecules to physiological function. *Annu Rev Physiol* 65:453–480.
2. Biel M, Zong X, Hofmann F (1996) Cyclic nucleotide-gated cation channels molecular diversity, structure, and cellular functions. *Trends Cardiovasc Med* 6(8):274–280.
3. Baruscotti M, Difrancesco D (2004) Pacemaker channels. *Ann N Y Acad Sci* 1015: 111–121.
4. Kaupp UB, Seifert R (2002) Cyclic nucleotide-gated ion channels. *Physiol Rev* 82(3): 769–824.
5. Craven KB, Zagotta WN (2006) CNG and HCN channels: Two peas, one pod. *Annu Rev Physiol* 68:375–401.
6. Zagotta WN, et al. (2003) Structural basis for modulation and agonist specificity of HCN pacemaker channels. *Nature* 425(6954):200–205.
7. Xu X, Vysotskaya ZV, Liu Q, Zhou L (2010) Structural basis for the cAMP-dependent gating in the human HCN4 channel. *J Biol Chem* 285(47):37082–37091.
8. Lolicato M, et al. (2011) Tetramerization dynamics of C-terminal domain underlies isoform-specific cAMP gating in hyperpolarization-activated cyclic nucleotide-gated channels. *J Biol Chem* 286(52):44811–44820.
9. Flynn GE, Black KD, Islas LD, Sankaran B, Zagotta WN (2007) Structure and rearrangements in the carboxy-terminal region of SpIH channels. *Structure* 15(6): 671–682.
10. Clayton GM, Silverman WR, Heginbotham L, Morais-Cabral JH (2004) Structural basis of ligand activation in a cyclic nucleotide regulated potassium channel. *Cell* 119(5): 615–627.
11. Clayton GM, Altieri S, Heginbotham L, Unger VM, Morais-Cabral JH (2008) Structure of the transmembrane regions of a bacterial cyclic nucleotide-regulated channel. *Proc Natl Acad Sci USA* 105(5):1511–1515.
12. Mari SA, et al. (2011) Gating of the MlotiK1 potassium channel involves large rearrangements of the cyclic nucleotide-binding domains. *Proc Natl Acad Sci USA* 108(51):20802–20807.
13. Nimigean CM, Shane T, Miller C (2004) A cyclic nucleotide modulated prokaryotic K^+ channel. *J Gen Physiol* 124(3):203–210.
14. Long SB, Campbell EB, Mackinnon R (2005) Crystal structure of a mammalian voltage-dependent Shaker family K^+ channel. *Science* 309(5736):897–903.
15. Brelidze TI, Carlson AE, Sankaran B, Zagotta WN (2012) Structure of the carboxy-terminal region of a KCNH channel. *Nature* 481(7382):530–533.
16. Brelidze TI, Gianulis EC, DiMaio F, Trudeau MC, Zagotta WN (2013) Structure of the C-terminal region of an ERG channel and functional implications. *Proc Natl Acad Sci USA* 110(28):11648–11653.
17. Marques-Carvalho MJ, et al. (2012) Structural, biochemical, and functional characterization of the cyclic nucleotide binding homology domain from the mouse EAG1 potassium channel. *J Mol Biol* 423(1):34–46.
18. Shi N, Ye S, Alam A, Chen L, Jiang Y (2006) Atomic structure of a Na^+- and K^+-conducting channel. *Nature* 440(7083):570–574.
19. Derebe MG, Zeng W, Li Y, Alam A, Jiang Y (2011) Structural studies of ion permeation and Ca^{2+} blockage of a bacterial channel mimicking the cyclic nucleotide-gated channel pore. *Proc Natl Acad Sci USA* 108(2):592–597.
20. Xu X, et al. (2012) Local and global interpretations of a disease-causing mutation near the ligand entry path in hyperpolarization-activated cAMP-gated channel. *Structure* 20(12):2116–2123.
21. Kuo MMC, Haynes WJ, Loukin SH, Kung C, Saimi Y (2005) Prokaryotic K^+ channels: From crystal structures to diversity. *FEMS Microbiol Rev* 29(5):961–985.
22. Kuo MM-C, Saimi Y, Kung C, Choe S (2007) Patch clamp and phenotypic analyses of a prokaryotic cyclic nucleotide-gated K^+ channel using *Escherichia coli* as a host. *J Biol Chem* 282(33):24294–24301.
23. Altschul SF, et al. (1997) Gapped BLAST and PSI-BLAST: A new generation of protein database search programs. *Nucleic Acids Res* 25(17):3389–3402.
24. Angelov A, et al. (2010) Genome sequence of the polysaccharide-degrading, thermophilic anaerobe *Spirochaeta thermophila* DSM 6192. *J Bacteriol* 192(24): 6492–6493.
25. Picardeau M, et al. (2008) Genome sequence of the saprophyte *Leptospira biflexa* provides insights into the evolution of *Leptospira* and the pathogenesis of leptospirosis. *PLoS One* 3(2):e1607.
26. Larkin MA, et al. (2007) Clustal W and Clustal X version 2.0. *Bioinformatics* 23(21): 2947–2948.
27. Drew D, Lerch M, Kunji E, Slotboom D-J, de Gier J-W (2006) Optimization of membrane protein overexpression and purification using GFP fusions. *Nat Methods* 3(4): 303–313.
28. Kawate T, Gouaux E (2006) Fluorescence-detection size-exclusion chromatography for precrystallization screening of integral membrane proteins. *Structure* 14(4):673–681.
29. Cortes DM, Perozo E (1997) Structural dynamics of the *Streptomyces lividans* K^+ channel (SKC1): Oligomeric stoichiometry and stability. *Biochemistry* 36(33): 10343–10352.
30. Rath A, Glibowicka M, Nadeau VG, Chen G, Deber CM (2009) Detergent binding explains anomalous SDS-PAGE migration of membrane proteins. *Proc Natl Acad Sci USA* 106(6):1760–1765.
31. Nache V, et al. (2012) Differential regulation by cyclic nucleotides of the CNGA4 and CNGB1b subunits in olfactory cyclic nucleotide-gated channels. *Sci Signal* 5(232):ra48.
32. Kaupp UB, et al. (1989) Primary structure and functional expression from complementary DNA of the rod photoreceptor cyclic GMP-gated channel. *Nature* 342(6251): 762–766.
33. Frings S, Lynch JW, Lindemann B (1992) Properties of cyclic nucleotide-gated channels mediating olfactory transduction. Activation, selectivity, and blockage. *J Gen Physiol* 100(1):45–67.
34. DiFrancesco D (1986) Characterization of single pacemaker channels in cardiac sino-atrial node cells. *Nature* 324(6096):470–473.
35. Dekker JP, Yellen G (2006) Cooperative gating between single HCN pacemaker channels. *J Gen Physiol* 128(5):561–567.
36. Thon S, Schmauder R, Benndorf K (2013) Elementary functional properties of single HCN2 channels. *Biophys J* 105(7):1581–1589.
37. Kusch J, Nache V, Benndorf K (2004) Effects of permeating ions and cGMP on gating and conductance of rod-type cyclic nucleotide-gated (CNGA1) channels. *J Physiol* 560(Pt 3):605–616.
38. Nache V, et al. (2005) Activation of olfactory-type cyclic nucleotide-gated channels is highly cooperative. *J Physiol* 569(Pt 1):91–102.
39. Maksaev G, Haswell ES (2011) Expression and characterization of the bacterial mechanosensitive channel MscS in *Xenopus laevis* oocytes. *J Gen Physiol* 138(6):641–649.
40. Bocquet N, et al. (2007) A prokaryotic proton-gated ion channel from the nicotinic acetylcholine receptor family. *Nature* 445(7123):116–119.
41. Choi SB, Kim J-U, Joo H, Min CK (2010) Identification and characterization of a novel bacterial ATP-sensitive K^+ channel. *J Microbiol* 48(3):325–330.
42. Nimigean CM, Pagel MD (2007) Ligand binding and activation in a prokaryotic cyclic nucleotide-modulated channel. *J Mol Biol* 371(5):1325–1337.
43. Biel M, Wahl-Schott C, Michalakis S, Zong X (2009) Hyperpolarization-activated cation channels: From genes to function. *Physiol Rev* 89(3):847–885.
44. Shabb JB, Corbin JD (1992) Cyclic nucleotide-binding domains in proteins having diverse functions. *J Biol Chem* 267(9):5723–5726.
45. Tibbs GR, Liu DT, Leypold BG, Siegelbaum SA (1998) A state-independent interaction between ligand and a conserved arginine residue in cyclic nucleotide-gated channels reveals a functional polarity of the cyclic nucleotide binding site. *J Biol Chem* 273(8): 4497–4505.
46. Chen S, Wang J, Siegelbaum SA (2001) Properties of hyperpolarization-activated pacemaker current defined by coassembly of HCN1 and HCN2 subunits and basal modulation by cyclic nucleotide. *J Gen Physiol* 117(5):491–504.
47. Altieri SL, et al. (2008) Structural and energetic analysis of activation by a cyclic nucleotide binding domain. *J Mol Biol* 381(3):655–669.
48. Young EC, Sciubba DM, Siegelbaum SA (2001) Efficient coupling of ligand binding to channel opening by the binding domain of a modulatory (beta) subunit of the olfactory cyclic nucleotide-gated channel. *J Gen Physiol* 118(5):523–546.
49. Chan KSC, Young EC (2009) Bimodal agonism in heteromeric cyclic nucleotide-gated channels. *Channels (Austin)* 3(6):427–436.
50. Wong W-F, Chan KSC, Michaleski MS, Haesler A, Young EC (2011) Ligand-binding domain subregions contributing to bimodal agonism in cyclic nucleotide-gated channels. *J Gen Physiol* 137(6):591–603.
51. Long SB, Campbell EB, Mackinnon R (2005) Voltage sensor of Kv1.2: Structural basis of electromechanical coupling. *Science* 309(5736):903–908.
52. Anselmi C, Carloni P, Torre V (2007) Origin of functional diversity among tetrameric voltage-gated channels. *Proteins* 66(1):136–146.

Supporting Information

Brams et al. 10.1073/pnas.1401917111

SI Experimental Procedures

Molecular Cloning and Protein Expression. National Center of Biotechnology Information reference numbers for protein sequences reported in this study are WP_009782512.1 (LpcK), YP_724331.1 (TerK), YP_003873862.1 (SthK), and YP_001962905.1 (LbiK). The GenBank reference number for AmaK is EDZ93391. Synthetic genes with optimized codon use for expression in *Escherichia coli* were purchased from Genscript. Each gene was subcloned into the NdeI and BamHI restriction sites of the vector pWaldo-GFPe (1, 2). Each plasmid was transformed into chemically competent OverExpress *E. coli* strains C41(DE3), C43(DE3), BL21 (DE3), and their pLysS variants (Lucigen). Bacterial suspension cultures were grown in Luria broth at a temperature of 37 °C to an optical density of 0.6–0.8 (OD_{600}). Protein expression was induced by addition of 400 μM isopropyl-thio-b-D-galactoside, and the cultures were subsequently cooled to 18 °C for overnight incubation. Cells were harvested by centrifugation at 10,000 × *g*, and the cell pellet was stored at −20 °C. Cell pellets were resuspended in lysis buffer containing 500 mM KCl, 50 mM Tris, pH 8.0, and 10% glycerol supplemented with 1 mM phenylmethanesulfonyl fluoride (PMSF), 20 mg/mL DNase, 5 mM $MgCl_2$, 1 μg/mL leupeptin, and 1 μg/mL pepstatin-A. Cells were broken by two passes at 1,000–1,500 bar through an Emulsiflex-C5 (Avestin). Membranes were isolated by ultracentrifugation in a Beckman Ti60 rotor at 125,000 × *g* at 4 °C for 1 h. Membranes were resuspended at a ratio of 1:1 (mass/vol) in buffer A, containing 500 mM KCl, 50 mM Tris, pH 8.0, and 10% glycerol supplemented with 1 mM PMSF. Membrane suspensions were snap frozen in liquid nitrogen before storage at −80 °C. Green fluorescence of GFP was monitored throughout this process using a Safe Imager blue light transilluminator (Invitrogen).

Expression and Detergent Screening. For initial expression screening, proteins were expressed in 4-mL suspension cultures under the same conditions as described above. Suspension cultures were harvested by centrifugation at 30,000 × *g* and resuspended in 400 μL of PBS. Whole-cell fluorescence was measured at room temperature in a 7500 Fast Real-Time PCR system (Applied Biosystems). For detergent screening, 270 μL of membrane suspension was mixed with 30 μL of a 20% detergent stock solution (final detergent concentration was 2% during solubilization). All detergents used in this study were obtained from Affymetrix. Next, the solubilized fraction was cleared by ultracentrifugation in a Beckman TLA 120.1 rotor at 30,000 × *g* at 4 °C for 1 h. The clear supernatant was further used for analysis by fluorescence size exclusion chromatography (FSEC) (1, 3). In brief, FSEC was carried out on a ÄKTApurifier 10 system (GE Healthcare Life Sciences) equipped with an A-900 autosampler, a Superose 6 10/300 GL column, and a RF-10AXL fluorescence detector (Shimadzu). Fluorescence of GFP was measured at an excitation wavelength of 488 nm and emission wavelength of 512 nm. Samples were run at 4 °C at a flow rate of 0.4 mL/min in running buffer containing buffer A supplemented with the corresponding detergent used during protein solubilization. Final detergent concentrations in running buffer were 0.02% Cymal-6, 0.6% lauryldimethylamine *N*-oxide (LDAO), 0.7% octyl glucoside (OG), 0.6% nonylglucoside (NG), 0.2% octylmaltoside (OM), 0.05% Fos-choline-12 (Fos-12), 0.2% decylmaltoside (DM), 0.15% undecylmaltoside (UDM), 0.05% dodecylmaltoside (DDM), 0.02% tridecylmaltoside (TDM), 0.1% lauryl maltose neopentyl glycol (LMNG), 0.05% C12E9, 0.1% CHAPS, and 0.3% HEGA-10.

Protein Purification. Total membrane preparations of channel-GFP-Hisx8 fusion constructs from 4- to 8-L suspension cultures were solubilized by stirring for 2 h at 4 °C in buffer A supplemented with detergent and 50 mM imidazole. Insoluble material was removed by ultracentrifugation at 30,000 × *g* at 4 °C for 1 h. The supernatant was loaded onto a 1-mL HisTrap FF column (GE Healthcare) and washed with two consecutive wash steps to 50 and 70 mM imidazole in buffer A. Protein was eluted with a linear gradient from 70 to 250 mM imidazole in buffer A. The flow through, wash, and elution fractions were analyzed using FSEC to verify the amount of channel-GFP-Hisx8 in each fraction. The main elution fractions were concentrated on a Vivaspin 6 (Sartorius) concentrating column (100-kDa cutoff), and the imidazole was exchanged by concentration/dilution before protease cleavage with 150 units of thrombin (Calbiochem) at 4 °C for 36 h. For the final gel filtration, the sample was loaded onto a Superdex 200 10/300 GL gel filtration column with running buffer composed of buffer A supplemented with 0.15% UDM for AmaK and 0.05% DDM for SthK. The final elution fractions were pooled and concentrated using a Vivaspin 6 concentrating column (100-kDa cutoff) and stored at 4 °C for further analysis.

Protein Analysis. Protein fractions were analyzed on 4–15% Mini-PROTEAN TGX precast SDS/PAGE gels (Bio-Rad). A Safe Imager blue light transilluminator (Invitrogen) was used to monitor in-gel GFP fluorescence. Precision Plus All Blue and Fluorescent WesternC Protein standards were from Bio-Rad. Gels were stained using the Coomassie R-250 method. Protein concentration was estimated using the Quick Start Bradford 1× dye reagent and an Eppendorf Bio spectrophotometer.

Expression in *Xenopus* oocytes. For oocyte expression studies, SthK was cloned as a C-terminal GFP fusion into the EcoRI and XbaI restriction sites of pGEM-HE (4, 5). All constructs were verified by sequencing (LGC Genomics). The plasmids were linearized with NheI, and capped cRNA was synthesized using the T7 mMESSAGE-mMACHINE transcription kit (Ambion). Oocytes were surgically removed from adult females of *Xenopus laevis* anesthetized with 0.3% 3-aminobenzoic acid ethyl ester. After incubating the oocytes for 105 min in Ca^{2+}-free Barth's solution (in mM: 82.5 NaCl, 2 KCl, 1 $MgCl_2$, and 5 Hepes, pH 7.5) containing 3 mg/mL collagenase A (Roche), oocytes of stage IV and V were manually dissected and defolliculated. About 50 ng of cRNA encoding SthK-GFP or AmaK-GFP per oocyte was injected. Oocytes were cultured at 18 °C for 3–5 d in Barth's medium [in mM: 84 NaCl, 1 KCl, 2.4 $NaHCO_3$, 0.82 $MgSO_4$, 0.41 $CaCl_2$, 0.33 $Ca(NO_3)_2$, 7.5 Tris, cefuroxime, and penicillin/streptomycin, pH 7.4]. The vitelline membrane was manually removed from the oocyte right before imaging or electrophysiological experiments.

Confocal Laser-Scanning Microscopy. Confocal fluorescence microscopy (LSM 710; Zeiss) was used to determine protein localization in the membrane of *Xenopus* oocytes. The fluorescence signal originating from SthK-GFP was identified using excitation with the 488-nm line of an argon laser. To confirm localization to the oocyte membrane, we stained the membrane with Alexa Fluor 633-labeled wheat germ agglutinin (WGA-Alexa 633) (Invitrogen Life Technologies) from the extracellular side (6). Staining was performed by removing the vitelline membrane and

incubating the oocytes for 10 min in bath solution containing 5 μM WGA-Alexa 633. Alexa 633 was excited with the 633-nm line of helium neon laser. The laser light was projected through a main beam splitter 488/543/633 and a Plan-Neofluar 10×/0.30 or a 40×/1.2 C-Apochromat water-immersion objective onto the sample. The emitted light was collected through the objective and spatially filtered by a 37-mm pinhole resulting in a *z* slice of 1 μm for the 40× objective and 12.8 μm for the 10× objective. To quantify colocalization of GFP and Alexa 633, we analyzed fluorescence profiles perpendicular to the plasma membrane (10 profiles averaged per oocyte and image). Both signals were normalized with respect to the integral of their profiles. The integral of the overlap between the two profiles was used as a quantitative measure of colocalization, indicating GFP membrane localization.

Spectral Imaging. To confirm that the emission spectrum obtained form SthK-GFP–expressing oocytes is GFP-related and not affected by autofluorescence, we recorded the autofluorescence spectrum of control oocytes and a GFP emission spectrum from HEK293 cells expressing cytosolic GFP. Control oocytes for autofluorescence imaging were harvested from *Xenopus laevis* as described in *Experimental Procedures*. HEK cells were transfected using the calcium phosphate transfection method. Excitation in oocytes and HEK cells was realized using the 488-nm line of an argon laser of the confocal laser-scanning microscope LSM710 (Zeiss). For SthK-GFP imaging, the applied laser power was 2.5 times lower than for autofluorescence imaging; thus, autofluorescence was not detectable in SthK experiments. Spectral detection was performed in the range of 472–686 nm for oocytes and in the range of 501–686 nm for HEK cells. The step width was 9.7 nm. In all cases, a Zeiss 40×/1.2-W Korr M27 objective was used.

Spectral imaging of AmaK-GFP–injected oocytes was performed in the same way as of SthK-GFP–injected oocytes, but with a 2.5 times higher laser power of the 488-nm line of an argon laser. For experiments performed to test the expression in *Xenopus* oocytes, the membrane was additionally counterstained with 5 μM WGA-Alexa 633.

Electrophysiology. Patch-clamp recordings were carried out in the inside-out configuration using macropatches excised from *Xenopus laevis* oocytes expressing SthK-GFP. Patch pipettes were pulled from borosilicate glass tubing (Hilgenberg) with outer and inner diameters of 2.0 and 1.0 mm, respectively. The resistance of the solution-filled pipettes was between 0.7 and 1.1 MΩ. The bath and the pipette solutions contained the following (in mM): 150 KCl, 5 EGTA, 5 Hepes (pH 7.4). In experiments upon the selectivity of SthK channels, KCl was substituted by 150 mM NaCl in the bath and/or pipette solution. All recordings were obtained at room temperature. Concentration–activation relationships for cAMP were obtained by applying different cAMP concentrations to the bath solution. Currents were recorded with an Axopatch 200B amplifier (Axon Instruments) controlled by the patch-clamp software ISO2 (MFK). Because of a run-up of the current amplitude in the first tens of seconds after ligand application, recordings were started 1 min after patch excision. For the experiments upon voltage dependence and ion selectivity of SthK, voltage steps of 2-s duration from −100 to +100 mV with 20-mV increments were applied. For cAMP concentration–activation relationships, the voltage was first stepped from a holding potential of 0 to −100 mV, then to +100 mV and back to the holding potential. The voltage steps lasted 2.1 s. Single-channel recordings were obtained under the same experimental conditions. All macroscopic currents were corrected for the capacitive and the leak components by subtracting respective currents in the absence of ligands in the bath solution. Concentration–activation relationships were determined from the steady-state current at +100 mV by normalizing the current I at the actual [cAMP] with respect to the current I_{max} at saturating [cAMP] and fitting the data points with a Hill equation of the following form:

$$\frac{I}{I_{max}} = \frac{1}{1 + \left(\frac{EC_{50}}{[cAMP]}\right)^{H}}, \qquad \textbf{[S1]}$$

yielding values for the concentration of half-maximum activation, EC_{50}, and the Hill coefficient, H. Curves were fitted to the data with appropriate nonlinear approximation algorithms using Origin9.0G (OriginLab Corporation) software. Single-channel analysis was performed using the ISO2 software (MFK). Amplitude histograms were fitted with the sum of Gaussian functions using Origin9.0G software (OriginLab Corporation). Statistical data are given as mean ± SEM.

1. Kawate T, Gouaux E (2006) Fluorescence-detection size-exclusion chromatography for precrystallization screening of integral membrane proteins. *Structure* 14(4):673–681.
2. Drew D, Lerch M, Kunji E, Slotboom D-J, de Gier J-W (2006) Optimization of membrane protein overexpression and purification using GFP fusions. *Nat Methods* 3(4):303–313.
3. Cortes DM, Perozo E (1997) Structural dynamics of the *Streptomyces lividans* K^+ channel (SKC1): Oligomeric stoichiometry and stability. *Biochemistry* 36(33): 10343–10352.
4. Rath A, Glibowicka M, Nadeau VG, Chen G, Deber CM (2009) Detergent binding explains anomalous SDS-PAGE migration of membrane proteins. *Proc Natl Acad Sci USA* 106(6):1760–1765.
5. Liman ER, Tytgat J, Hess P (1992) Subunit stoichiometry of a mammalian K^+ channel determined by construction of multimeric cDNAs. *Neuron* 9(5):861–871.
6. Nache V, et al. (2012) Differential regulation by cyclic nucleotides of the CNGA4 and CNGB1b subunits in olfactory cyclic nucleotide-gated channels. *Sci Signal* 5(232):ra48.

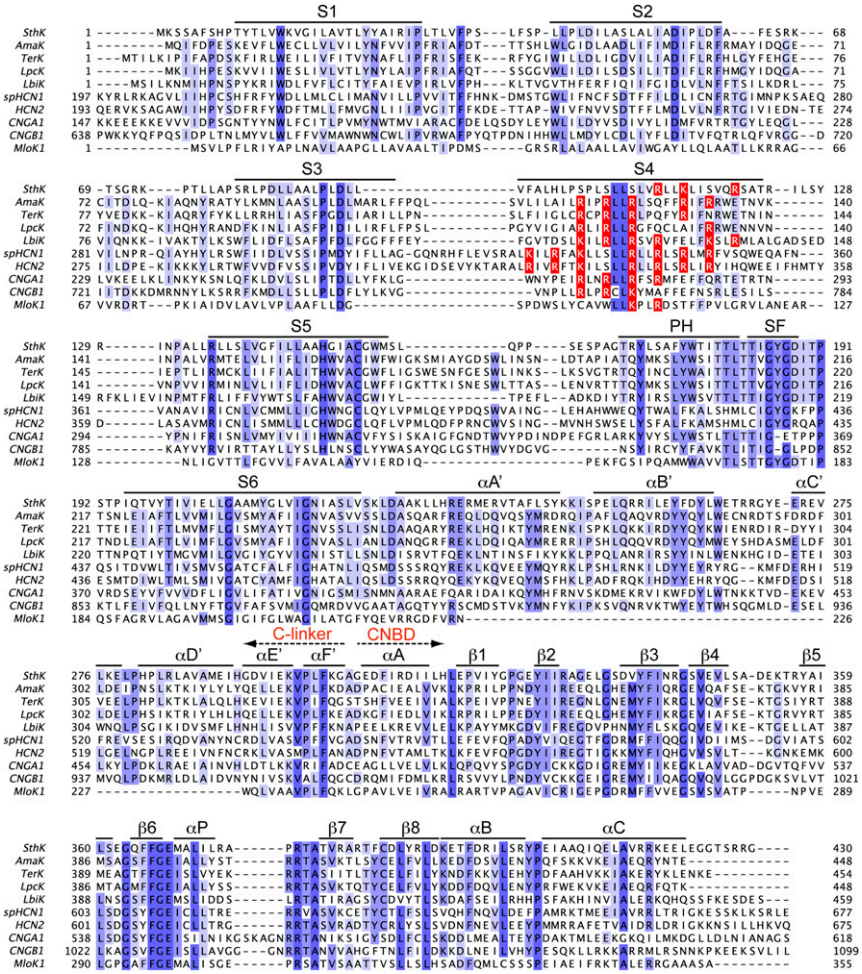

Fig. S1. Full-sequence alignment of prokaryote cyclic nucleotide-modulated ion channels with different eukaryote HCN and CNG channels.

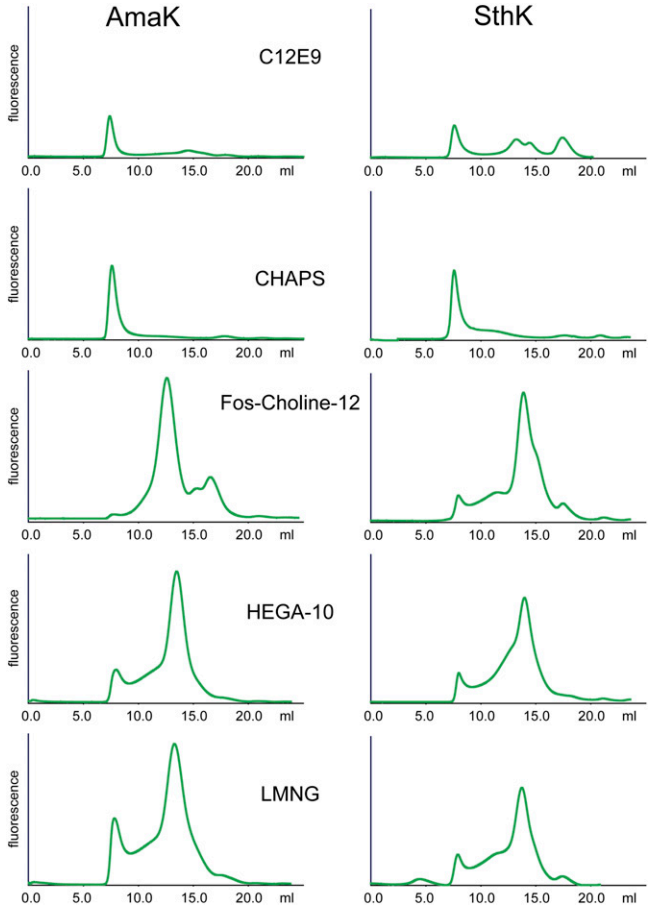

Fig. S2. Detergent screen for AmaK and SthK using FSEC. FSEC profiles show that C12E9 and CHAPS are unable to stably extract AmaK or SthK from membranes. For Fos-12, HEGA-10, and LMNG, relatively symmetric fluorescent peaks could be observed, indicating that AmaK and SthK are extracted from membranes in a monodisperse state.

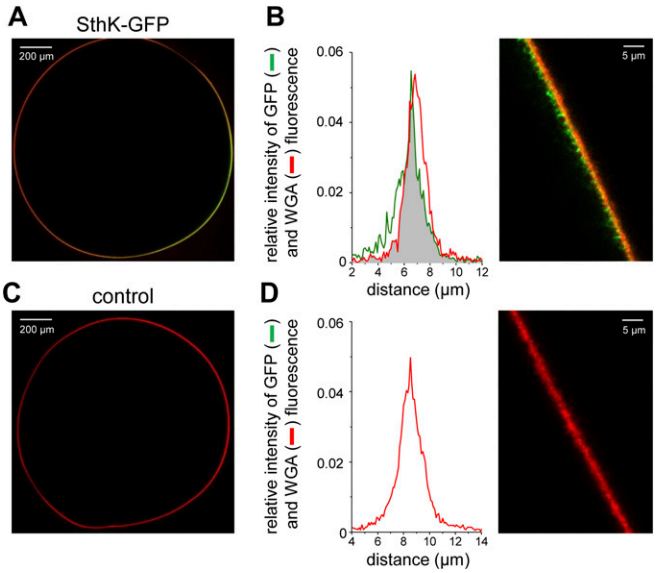

Fig. S3. Membrane localization of SthK-GFP in *Xenopus* oocytes. (*A*) Confocal image of an intact oocyte expressing SthK-GFP. The outer side of the membrane was counterstained with WGA-Alexa 633 to define the position of the membrane (red signal). GFP emission signal is shown in green. Shades of yellow are caused by superimposed red and green signals. (*B*) Confocal image of an oocyte expressing SthK-GFP at higher magnification. The fluorescence profiles are averages of 10 profiles perpendicular to the membrane surface for GFP (green) and Alexa 633 (red). Normalization of the profiles was performed by setting the area under the curves to unity. The gray area marks the portion of colocalization. (*C*) Confocal image of an intact noninjected control oocyte. Counterstaining the outer side of the membrane caused a red signal similar to *A*. A green signal is missing due to the absence of SthK-GFP. There was no autofluorescence signal under these experimental conditions. (*D*) Confocal image of a control oocyte at higher magnification. The fluorescence of the Alexa 633 profile is similar to SthK-GFP–expressing oocytes, shown in *B*.

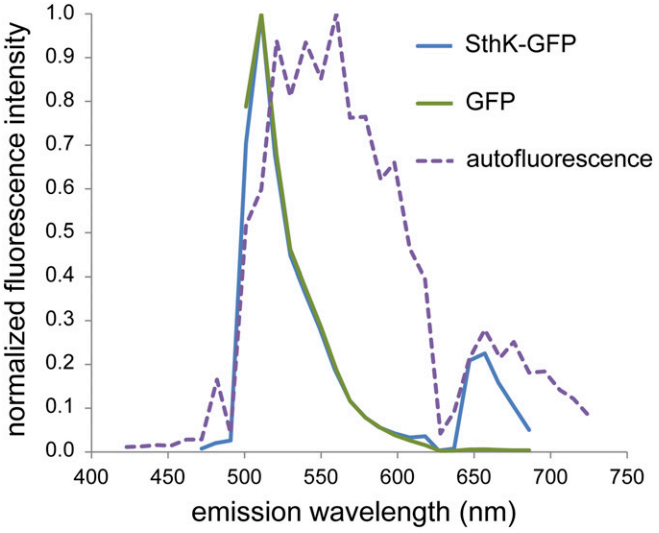

Fig. S4. Comparison of emission spectra for SthK-GFP, cytosolic GFP, and autofluorescence. Shown are the emission spectra of SthK-GFP expressed in *Xenopus laevis* oocytes, cytosolic GFP expressed in HEK293 cells, and the spectrum of the autofluorescence in control oocytes. All three emission spectra were normalized with respect to the maximum values for comparison. The superimposition of the SthK-GFP and GFP spectra indicates that the spectrum recorded in SthK-GFP–expressing oocytes is not affected by autofluorescence.

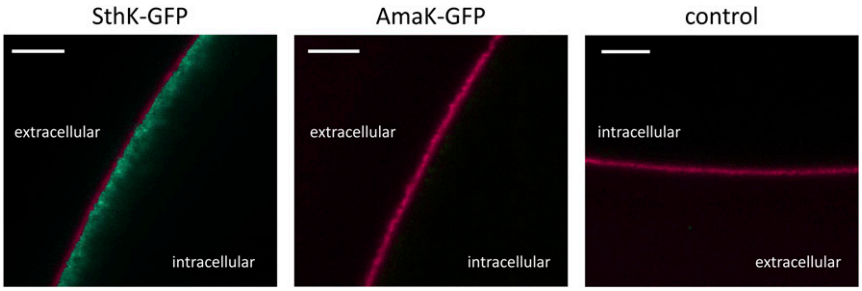

Fig. S5. Spectral imaging of *Xenopus laevis* oocytes. Shown are spectral images (*SI Experimental Procedures*) of oocytes 3 d after injection of SthK-GFP and AmaK-GFP cRNA, respectively, in comparison with a noninjected control oocyte. Whereas in SthK-GFP oocytes a strong GFP fluorescence could be detected, there was no GFP-related signal in AmaK-GFP or control oocytes. The red fluorescence arose from WGA-Alexa 633 counterstaining to confirm the position of the plasma membrane (*SI Experimental Procedures*). (Scale bar: 20 μM in all three images.)